Physica E 127 (2021) 114491

Contents lists available at ScienceDirect

Physica E: Low-dimensional Systems and Nanostructures

journal homepage: http://www.elsevier.com/locate/physe

Magneto-optical transport properties of parabolic potential GaAs/$Ga_{1-\kappa}Al_{\kappa}As$ wells under the influence of Al concentration and hydrostatic pressure

Le Thi Quynh Huong [a,b], Le Ngoc Minh [c], Nguyen Thi Xuan Hoai [d], Nguyen Dinh Hien [e,f,*]

[a] Institute of Research and Development, Duy Tan University, Danang, 550000, Viet Nam
[b] Faculty of Natural Sciences, Duy Tan University, Danang, 550000, Viet Nam
[c] Faculty of Physics, University of Sciences, Hue University, Hue City, Viet Nam
[d] Department of Physics, University of Education, The University of Danang, Da Nang, Viet Nam
[e] Laboratory of Magnetism and Magnetic Materials, Advanced Institute of Materials Science, Ton Duc Thang University, Ho Chi Minh City, Viet Nam
[f] Faculty of Applied Sciences, Ton Duc Thang University, Ho Chi Minh City, Viet Nam

ARTICLE INFO

Keywords:
GaAs/$Ga_{1-\kappa}Al_{\kappa}As$ PQWs
Hydrostatic pressure
Aluminum concentration
Confined modes

ABSTRACT

Magneto-optical transport properties of GaAs/$Ga_{1-\kappa}Al_{\kappa}As$ parabolic potential quantum-wells (PQWs) under the effects of Al-contents, hydrostatic pressure, and temperature is examined by studying their effects on the absorption power (AP) for magnetophonon resonance (MPR) and on the full width at half maximum (FWHM) of the optically-detected-MPR (ODMPR) peak due to modes confinement represented by slab-mode model, Huang-Zhu (HZ) model, guided-mode model. The numerical results indicate the Al-contents, pressure, as well as temperature which have great effect on the AP and FWHM in PQWs. Moreover, the results are also compared to bulk phonon modes for both two processes of phonons (emission and absorption). The results denote that phonon absorption process is always much more dominant compared to phonon emission process for four types of above phonons. In particular, the influences of pressure, Al-concentration in $Ga_{1-\kappa}Al_{\kappa}As$ barriers on the magneto-phonon resonance AP and FWHM in PQWs are more pronounced as confined modes are taken into account.

1. Introduction

The considerable development of semiconductor structures deposition technologies have led to unusual wells for instance, the triangular potential wells and parabolic potential wells. The parabolic-potential wells have considerable difference from square-potential wells, wherefore the parabolic wells have received significant interest of many theoretical and experimental physicists in the past few years [1,2]. Two-dimensional (2D) structure is one of the material structures has been interested significantly in recent years, most of the considerations on materials have been carried out on semiconductors for material III-V, among them, the $Ga_{1-\kappa}Al_{\kappa}As$/GaAs material heterostructures is noticeable. One of the reasons of this is the optical properties of this $Ga_{1-\kappa}Al_{\kappa}As$/GaAs semiconductor heterostructures are of fair importance in possible optoelectronic device application [3–8]. The alloy $Ga_{1-\kappa}Al_{\kappa}As$/GaAs system is a useful material for many photonic and optoelectronic devices with high speed because of GaAs material has insignificant difference from the lattice parameter of $Ga_{1-\kappa}Al_{\kappa}As$ material, and at system's temperature about 300 K it may be neglected, this promises an insignificant concentration of states of inexpedient interface. Besides, the optoelectronic natures of these heterostructures largely change as it be scaled down to single or one little atomic layers [9,10]. Alloy-composition-dependence of band gap energy for material $Ga_{1-\kappa}Al_{\kappa}As$ is one of the most necessary structural parameters of devices for technology of nano semiconductor and it has attracted the attention of physicists [11]. Moreover, 2D electrons systems have received significant interest is because of the tunable wide band gap energy and vigorous confinement of them [12,13]. To have realistic estimates for electron–optical-phonon scattering intensity we should consider under the influence of the confined optical modes in wells, because it plays an important roles for change the state density for optical phonon in low-dimensional structures whenever the width of the well, L_z, being

* Corresponding author. Laboratory of Magnetism and Magnetic Materials, Advanced Institute of Materials Science, Ton Duc Thang University, Ho Chi Minh City, Viet Nam.
E-mail addresses: letquynhhuong1@duytan.edu.vn (L.T.Q. Huong), nguyendinhhien@tdtu.edu.vn (N.D. Hien).

https://doi.org/10.1016/j.physe.2020.114491
Received 6 May 2020; Received in revised form 17 August 2020; Accepted 2 October 2020
Available online 21 October 2020

smaller than the phonon coherence length. Also, the physical natures of the electrons and phonons confinement have a considerable difference, for instance the confinement of phonons is because of the reflection of phonons-wave at the heterointerfaces of layers of semiconductor, while that of electrons caused by the reflection at the electric potential barriers of electron gas [14–17]. This physical nature of confined phonon modes can lead to a increase in electrophonon scattering possibility wherefore the FWHM of the peak enhances. The FWHM is known to be sensitive to the type of scattering-mechanisms effecting on the electron transport behaviors [18–20], and as the profile of the curve represents the dependence of $\hbar\omega$ on AP [18,21]. Therefore, it is a good tool to consider the electrons scattering mechanism in semiconductor heterostructures. According to this definition, our group has found a technique, and it can be called the profile method [22]. Utilizing this technique we obtain FWHMs of peaks from graphs of AP. This technique has been applied successfully for some works in low-dimensional semiconductor structures [23–31] as well as monolayer materials [32–34]. The study of the absorption FWHM we can directly observe magneto-phonon resonance (MPR) which is defined to be because of the resonance scattering of electron between LLs (Landau levels) along with phonon bsorption (emission), this effect occurs as separation of two LLs being equal to energy of LO-phonon [35,36]. This observation is called ODMPR [35, 37]. In other to obtain useful information on band structure parameters of material as well as scattering mechanisms of carriers in low-dimensional structural semiconductors, the ODMPR effect should be considered [35,38]. The combined effect of temperature, Al contents, and hydrostatic pressure is a good tool to modify the effective mass of the electron, band structure, confined potential, as well as dielectric constant and they lead to modify in the property of elementary excitation in heterostructures [39,40]. These combined effects due to the electrophonon scattering have been theoretically investigated previously in quantum wells [39,40], superlattices [41], and quantum wire [42]; as well as experimentally studied [43]. However, these studies was only considered under the effect of bulk modes. Therefore, further investigation is necessary to understand the combined influences of Al contents, temperature, as well as pressure on absorption AP as well as FWHMs of ODMPR peaks for GaAs/$Ga_{1-\kappa}Al_\kappa$As parabolic-potential wells as confined modes are taken into account. The obtained results can resupply good information in field of the electronic-devices and optoelectronic-devices fabrication. The organization of paper is as follows. Electron–bulk and confined phonons interaction in parabolic potential GaAs/$Ga_{1-\kappa}Al_\kappa$As wells is calculated in Sec. 2. Absorption power in parabolic potential GaAs/$Ga_{1-\kappa}Al_\kappa$As wells under the influences of the Al contents, temperature, and hydrostatic pressure, and is obtained in Sec. 3. Sec. 4 will be result and discussion. Sec. 5 is devoted to conclusion.

2. Electron–bulk and confined phonons interaction in parabolic potential GaAs/$Ga_{1-\kappa}Al_\kappa$As quantum wells

We consider a GaAs/$Ga_{1-\kappa}Al_\kappa$As well with parabolic confinement potential $V(z) = m^*(\kappa,P,T)\omega_z^2 z^2/2$, in which electrons in the z-direction, they are confined through confinement potential $V(z)$ while free in the (x, y)-directions. With magnetic field, $\vec{B}$, is in the z-axis, the eigenfunctions and eigenvalue are given as [2,44–46].

$$\Psi_{N,n,k_y}(\vec{r}) = \frac{1}{\sqrt{L_y}}\exp(ik_y y)\psi_N(x-x_0)\phi_n(z), \tag{1}$$

$$E_{N,n,\kappa,p,T} = (N+\frac{1}{2})\hbar\omega_c(\kappa,P,T) + (n+\frac{1}{2})\hbar\omega_z, \tag{2}$$

where ψ_N is referred to as the harmonic oscillator function, centered at $x_0 = -a_c^2 k_y$, ω_z is the electron confining frequency. N and a_c denote the LLs and the cyclotron radius, where $N = 0, 1, \ldots$and $a_c = \sqrt{\hbar c/(eB)}$. The cyclotron frequency is symbolled to be $\omega_c(\kappa, P, T) = eB/m^*(\kappa, P, T)$. L_y and k_y respectively denote the normalization-length and wave-vector along the y-axis. For parabolic confinement potential, the corresponding eigenfunction $\phi_n(z)$ for electron along z-direction can be described by the expression as below

$$\phi_n(z) = \frac{1}{\sqrt{2^n n!\sqrt{\pi}a_z}}\exp(-\frac{z^2}{2a_z^2})H_n(\frac{z}{a_z}), \tag{3}$$

with H_n are Hermite polynomials, and $a_z = (\hbar/(m^*\omega_z))^{1/2}$.

Where $m^*(\kappa, P, T)$ is referred to as the effective mass, and it has a vigorous dependence on the Al-contents κ, temperature of system T, and hydrostatic pressure P, and it is described by Refs. [31,39,42].

$$m^*(\kappa,P,T) = \frac{m_0}{1+\frac{\Pi^2(\kappa)}{3}\left(\frac{2}{E_g^\Gamma(\kappa,P,T)}+\frac{1}{E_g^\Gamma(\kappa,P,T)+\vartheta(\kappa)}\right)+\Theta(\kappa)}, \tag{4}$$

where m_0 is referred to as the free electron mass. $E_g^\Gamma(\kappa, P, T)$ is the energy gap function for point Γ in the Brillouin zone, and it is given as [31,39].

$$E_g^\Gamma(\kappa,P,T) = \mu_1 + \mu_2\kappa + \mu_3\kappa^2 + \zeta P - \frac{\sigma T^2}{\upsilon + T}, \tag{5}$$

where $\mu_1 = 1519.4$ (meV), $\mu_2 = 1360$ (meV), $\mu_3 = 220$ (meV), $\zeta = 107$ meV $(\text{GPa})^{-1}$. $\Theta(\kappa) = -3.935 + 0.488\kappa + 4.938\kappa^2$ is referred to as the remote band effects. $\sigma = 0.5405$ meV K^{-1}, $\vartheta(\kappa) = 314 - 6\kappa$ (meV) represents the valence band spin orbit splitting, in which $\upsilon = 204$ K. $\Pi(\kappa) = \sqrt{28900 - 6290\kappa}$ (meV) refers to the inter-band matrix element.

2.1. In the case where electron is scattered by bulk optical phonon

The matrix element of electrophonon interaction because of bulk phonon is expressed by [18,47–51].

$$|\langle i|H_{e-ph}^{bulk}|f\rangle|^2 = |V_q(\kappa,P,T)|^2|I_{nn'}(q_z)|^2|J_{NN'}(u)|^2\delta_{k'_\perp,k_\perp\pm q_\perp}, \tag{6}$$

where the term $V_q(\kappa, P, T)$ represents the coupling factor, and is given by

$$|V_q(\kappa,P,T)|^2 = \frac{e^2\hbar\omega_{LO}(\kappa)\chi^*(\kappa,P,T)}{2\varepsilon_0 V_0(q_\perp^2+q_z^2)} \tag{7}$$

for optical phonon modes. Where $-e$ is the electron charge, $V_0 = SL_z$. The term $I_{nn'}(q_z)$ is the overlap integral over dz and is describe by the expression as follows

$$I_{nn'}(q_z) = \int_{-\infty}^{\infty}\phi_n(z)\exp(iq_z z)\phi_{n'}(z)dz, \tag{8}$$

and $J_{NN'}(u)$ is given by expression below

$$|J_{NN'}(u)|^2 = \frac{n_2!e^{-u}u^{n1-n2}}{n_1!}[L_{n2}^{n1-n2}(u)]^2, \tag{9}$$

where $L_{n2}^{n1-n2}(u)$ denotes the Laguerre polynomial, and $n1 \equiv \max\{N, N'\}$, $u = (a_c q_\perp)^2/2$, and $n2 \equiv \min\{N, N'\}$. Also, ε_0 is referred to be vacuum dielectric constant.

In GaAs/$Ga_{1-\kappa}Al_\kappa$As quantum wells with parabolic confinement potential, the longitudinal optical (LO) mode energy depends on the

aluminum concentration κ is represented by $\hbar\omega_{LO} = 36.25 + 1.83\kappa + 17.12\kappa^2 - 5.11\kappa^3$ (meV) [11,31,52]. Moreover, $\chi_0(P, T)$ denotes the static dielectric constant, and it is presented by [31,42].

$$\chi_0(P,T) = \begin{cases} \lambda_1 \exp[-\tau P + \xi_1(T - T_1)] & \text{for } T < 200 \text{ K}, \\ \lambda_2 \exp[-\tau P + \xi_2(T - T_2)] & \text{for } T \geq 200 \text{ K}, \end{cases} \tag{10}$$

with $\tau = 1.73 \times 10^{-2}$ 1/GPa, $\xi_1 = 9.4 \times 10^{-5}\,\text{K}^{-1}$, $\xi_2 = 20.4 \times 10^{-5}\,\text{K}^{-1}$, $T_1 = 75.6$ K, $T_2 = 300$ K, $\lambda_1 = 12.47$, and $\lambda_2 = 13.18$. Also, $\chi_\infty(\kappa, P, T)$ is referred to as the high-frequency dielectric constant, it is given by [11, 31].

$$\chi_\infty(\kappa, P, T) = -2.73\kappa + 10.89, \tag{11}$$

and then, we set

$$\chi^*(\kappa, P, T) = -\frac{1}{\chi_0(P,T)} + \frac{1}{\chi_\infty(\kappa, P, T)}. \tag{12}$$

2.2. In the case where electron–confined mode scattering

When electron is scattered by confined mode described by HZ model, slab modes, guided modes with the interaction matrix element is expressed as follows [53–58].

$$|\langle i|H^{conf.}_{e-ph}|f\rangle|^2 = \frac{e^2\chi^*(\kappa,P,T)}{2\varepsilon_0 V_0}\frac{\hbar\omega^{\ell,q_\perp}_{LO}|Y^{\ell\theta}_{nn'}(z)|^2}{a_{\ell\theta}q_\perp^2 + b_{\ell\theta}/L_z^2}|J_{NN'}(u)|^2|\delta_{k'_\perp,k_\perp\pm q_\perp}, \tag{13}$$

where, the term $Y^{\ell\theta}_{nn'}(z)$ is the overlap integral over dz, where it is written by

$$Y^{\ell\theta}_{nn'}(z) = \int_{-\infty}^{\infty} dz\phi^*_{n'}(z)\nu_{\ell\theta}(z)\phi_n(z), \tag{14}$$

with $\nu_{\ell\theta}(z)$ denotes the composition along parallel direction of the displacement vector of confined mode ℓth. Also, $\theta = +$, $\theta = -$ which refer to odd modes, even modes, respectively. The term $\nu_{\ell\theta}(z)$ is given by the expressions as

$$\begin{aligned} \nu_{\ell+}(z) &= \sin\left(\frac{\varsigma_\ell\pi z}{L_z}\right) + \frac{c_\ell z}{L_z}, \ \ell = 3,5,7,\ldots, \\ \nu_{\ell-}(z) &= \cos\left(\frac{\varsigma_\ell\pi z}{L_z}\right) - (-1)^{\ell/2}, \ \ell = 2,4,6,\ldots, \end{aligned} \tag{15}$$

for HZ model, and

$$\begin{aligned} \nu_{\ell+}(z) &= \cos\left(\frac{\ell\pi z}{L_z}\right), \ \ell = 1,3,5,\ldots, \\ \nu_{\ell-}(z) &= \sin\left(\frac{\ell\pi z}{L_z}\right), \ \ell = 2,4,6,\ldots, \end{aligned} \tag{16}$$

for slab modes, and

$$\begin{aligned} \nu_{\ell+}(z) &= \sin\left(\frac{\ell\pi z}{L_z}\right), \ \ell = 1,3,5,\ldots, \\ \nu_{\ell-}(z) &= \cos\left(\frac{\ell\pi z}{L_z}\right), \ \ell = 2,4,6,\ldots, \end{aligned} \tag{17}$$

for the guided modes.

Also, for HZ model, the factors $a_{\ell\theta}$ and $b_{\ell\theta}$ are expressed as follows

$$a_{\ell+} = 1 + c_\ell^2\left(\frac{1}{6} - \frac{1}{\varsigma_\ell^2\pi^2}\right), b_{\ell+} = \varsigma_\ell^2\pi^2 - c_\ell^2, \ \ell = 3,5,7,\ldots, \tag{18}$$

where ς_ℓ, c_ℓ are described by

$$\tan\left(\frac{\varsigma_\ell\pi}{2}\right) = \frac{\varsigma_\ell\pi}{2}, c_\ell = -2\sin\left(\frac{\varsigma_\ell\pi}{2}\right), \ \ell - 1 < \varsigma_\ell < \ell, \tag{19}$$

$$a_{\ell-} = 3, b_{\ell-} = \ell^2\pi^2, \ \ell = 2,4,6,\ldots. \tag{20}$$

These factors respectively are

$$a^{FK,R}_{\ell\pm} = 1, b^{FK,R}_{\ell\pm} = \ell^2\pi^2, \ \ell = 1,2,3,\ldots, \tag{21}$$

for guided and slab modes.

3. Absorption power in parabolic potential GaAs/$Ga_{1-\kappa}Al_\kappa$As wells under the combined influences of Al contents, temperature, and hydrostatic pressure

We calculate the AP in GaAs/$Ga_{1-\kappa}Al_\kappa$As quantum-wells with parabolic potential subjected to an electromagnetic wave by using the bulk mode and confinement mode. The expression of the AP is given by Ref. [59]:

$$AP(\omega,\kappa,P,T) = \frac{E_0^2}{2\omega}\sum_\alpha |j^+_\alpha(\kappa,P,T)|^2 \frac{[f_\alpha(\kappa,P,T) - f_{\alpha+1}(\kappa,P,T)]\hbar[\Gamma_\alpha(\omega,\kappa,P,T)]}{[\hbar\omega - \hbar\omega_c(\kappa,P,T)]^2 + [\hbar\Gamma_\alpha(\omega,\kappa,P,T)]^2}, \tag{22}$$

where electromagnetic wave with amplitude and frequency respectively are E_0 and ω, and the quantity, $j^+_\alpha(\kappa,P,T)$, is given by

$$|j^+_\alpha(\kappa,P,T)|^2 = (N+1)2e^2\hbar\omega_c(\kappa,P,T)\Big/m^*(\kappa,P,T), \tag{23}$$

$f_\alpha(\kappa, P, T)$ and $f_{\alpha+1}(\kappa, P, T)$ are respectively the Fermi-Dirac distribution functions for electron at state α and state $\alpha + 1$.

3.1. For bulk optical phonon modes

When electron is scattered by bulk mode, the term $\Gamma_\alpha(\omega, \kappa, P, T)$ in expression (22) is expressed by

$$\begin{aligned} \Gamma_\alpha(\kappa,P,T,\omega) &\equiv \Gamma^b_\alpha(\kappa,P,T,\omega) \\ &= \frac{e^2\chi^*(\kappa,P,T)\hbar\omega_{LO}(\kappa)}{8\pi^2\hbar\varepsilon_0}\sum_{N'}\sum_{n'}G_{nn'}\frac{1}{[f_{N+1,n}(\kappa,P,T) - f_{N,n}(\kappa,P,T)]} \\ &\times\int_0^\infty\left\{Y_1\delta[E_1^-(\kappa,P,T)] + Y_2\delta[E_1^+(\kappa,P,T)]\right\}\frac{|J_{N,N'}(u)|^2}{q_\perp}dq_\perp \\ &+\frac{e^2\chi^*(\kappa,P,T)\hbar\omega_{LO}(\kappa)}{8\pi^2\hbar\varepsilon_0}\sum_{N'}\sum_{n'}G_{nn'}\frac{1}{[f_{N+1,n}(\kappa,P,T) - f_{N,n}(\kappa,P,T)]} \\ &\times\int_0^\infty\left\{Y_3\delta[E_2^-(\kappa,P,T)] + Y_4\delta[E_2^+(\kappa,P,T)]\right\}\frac{|J_{N+1,N'}(u)|^2}{q_\perp}dq_\perp, \end{aligned} \tag{24}$$

where

$$\begin{aligned} G_{nn'} &= \int_{-\infty}^{\infty}|I_{nn'}(q_z)|^2dq_z = \frac{\sqrt{2}(1+\Delta n)_n(2\Delta n + \frac{3}{2})_n\Gamma(\Delta n + \frac{1}{2})}{a_z n!n'!} \\ &\times{}_3\Phi_2(-n, \Delta n + \frac{1}{2}, \frac{1}{2}; \Delta n + 1, \frac{1}{2} - n; 1), \end{aligned} \tag{25}$$

where ${}_3\Phi_2(-n, \Delta n + \frac{1}{2}, \frac{1}{2}; \Delta n + 1, \frac{1}{2} - n; 1)$ is the hypergeometric function, $\Delta n = n' - n$, here

$$ {}_3\Phi_2(a,b,c;d,g;h) = \sum_{j=0}^{\infty} \frac{(a)_j (b)_j (c)_j h^j}{(d)_j (g)_j j!}, \tag{26} $$

in which Pochhammer's symbol $(a)_i$ is described by

$$ (b)_j = b(b+1)\cdots(b+j-1) = \Gamma(b+j)/\Gamma(b). \tag{27} $$

$$ \begin{aligned} Y_1 \quad &= [1+N_q^-(\kappa)] f_{N+1,n}(\kappa,P,T)[1-f_{N',n'}(\kappa,P,T)] \\ &\quad -N_q^-(\kappa) f_{N',n'}(\kappa,P,T)[1-f_{N+1,n}(\kappa,P,T)], \end{aligned} \tag{28} $$

$$ \begin{aligned} Y_2 \quad &= N_q^-(\kappa) f_{N+1,n}(\kappa,P,T)[1-f_{N',n'}(\kappa,P,T)] - \\ &\quad [1+N_q^-(\kappa)] f_{N',n'}(\kappa,P,T)[1-f_{N+1,n}(\kappa,P,T)], \end{aligned} \tag{29} $$

$$ \begin{aligned} Y_3 \quad &= [1+N_q^-(\kappa)] f_{N',n'}(\kappa,P,T)[1-f_{N,n}(\kappa,P,T)] - N_q^-(\kappa) f_{N,n}(\kappa,P,T)[1 \\ &\quad -f_{N',n'}(\kappa,P,T)], \end{aligned} \tag{30} $$

$$ \begin{aligned} Y_4 \quad &= N_q^-(\kappa) f_{N',n'}(\kappa,P,T)[1-f_{N,n}(\kappa,P,T)] - [1+N_q^-(\kappa)] f_{N,n}(\kappa,P,T)[1 \\ &\quad -f_{N',n'}(\kappa,P,T)], \end{aligned} \tag{31} $$

$$ \begin{aligned} E_1^{\pm}(\kappa,P,T) \quad &= \quad \hbar\omega + (n^{'}-n)\hbar\omega_z + (N^{'}-N-1)\hbar\omega_c(\kappa,P,T) \\ &\quad \pm\hbar\omega_{LO}(\kappa), \end{aligned} $$

$$ E_2^{\pm}(\kappa,P,T) = \hbar\omega + (n-n^{'})\hbar\omega_z + (N-N^{'})\hbar\omega_c(\kappa,P,T) \pm \hbar\omega_{LO}(\kappa). \tag{32} $$

Where the Dirac delta functions $\delta\left(E_1^{\pm}(\kappa,P,T)\right), \delta\left(E_2^{\pm}(\kappa,P,T)\right)$ in Eq. (24) are replaced by width Lorentzians $\gamma_{N,N'}^{\pm,b}(\kappa,P,T), \gamma_{N+1,N'}^{\pm,b}(\kappa,P,T)$ as follows [60]:

$$ \delta\left(E_1^{\pm}(\kappa,P,T)\right) = \frac{\gamma_{N,N'}^{\pm}(\kappa,P,T)}{\pi\left\{\left[E_1^{\pm}(\kappa,P,T)\right]^2 + \left[\gamma_{N,N'}^{\pm}(\kappa,P,T)\right]^2\right\}}, \tag{33} $$

$$ \delta\left(E_2^{\pm}(\kappa,P,T)\right) = \frac{\gamma_{N+1,N'}^{\pm}(\kappa,P,T)}{\pi\left\{\left[E_2^{\pm}(\kappa,P,T)\right]^2 + \left[\gamma_{N+1,N'}^{\pm}(\kappa,P,T)\right]^2\right\}}, \tag{34} $$

where

$$ \left[\gamma_{N',N}^{\pm}(\kappa,P,T)\right]^2 = \frac{e^2\hbar\omega_{LO}(\kappa)\chi^*(\kappa,P,T)}{8\pi^3\hbar^2\varepsilon_0 S}\left[N_q^-(\kappa)+\frac{1}{2}\pm\frac{1}{2}\right]G_{nn'}\int_0^{\infty} dq_{\perp}\frac{|J_{N,N'}(u)|^2}{q_{\perp}}, \tag{35} $$

$$ \left[\gamma_{N+1,N'}^{\pm}(\kappa,P,T)\right]^2 = \frac{e^2\hbar\omega_{LO}(\kappa)\chi^*(\kappa,P,T)}{8\pi^3\hbar^2\varepsilon_0 S}\left[N_q^-(\kappa)+\frac{1}{2}\pm\frac{1}{2}\right]G_{nn'}\int_0^{\infty} dq_{\perp}\frac{|J_{N+1,N'}(u)|^2}{q_{\perp}}. \tag{36} $$

3.2. For confined optical phonon modes

When electron is scattered by confined mode, the term $\Gamma_\alpha(\omega, \kappa, P, T)$ in Eq. (22) is expressed as below

$$ \begin{aligned} &\Gamma_\alpha(\omega,\kappa,P,T) \equiv \Gamma_\alpha^c(\omega,\kappa,P,T) \\ &= \frac{e^2}{8\pi\hbar\varepsilon_0 L_z}\sum_{\ell}\sum_{\theta=\pm}\sum_{N',n'}\hbar\omega_{LO}^{\ell,q_\perp}(\kappa)\chi^*(\kappa,P,T) \\ &\quad \frac{|\Upsilon_{nn'}^{\ell\theta}|^2}{[f_{N+1,n}(\kappa,P,T)-f_{N,n}(\kappa,P,T)]} \\ &\quad \times\int_0^{\infty}\left\{Y_1\delta[E_1^-(\kappa,P,T)]+Y_2\delta[E_1^+(\kappa,P,T)]\right\}\frac{q_\perp|J_{N,N'}(u)|^2}{a_{\ell\eta}^{\lambda}q_\perp^2+\frac{b_{\ell\eta}^{\lambda}}{L_z^2}}dq_\perp \\ &\quad \frac{e^2}{8\pi\hbar\varepsilon_0 L_z}\sum_{\ell}\sum_{\theta=\pm}\sum_{N',n'}\hbar\omega_{LO}^{\ell,q_\perp}(\kappa)\chi^*(\kappa,P,T) \\ &\quad \frac{|\Upsilon_{nn'}^{\ell\theta}|^2}{[f_{N+1,n}(\kappa,P,T)-f_{N,n}(\kappa,P,T)]} \\ &\quad \times\int_0^{\infty}\left\{Y_3\delta[E_2^-(\kappa,P,T)]+Y_4\delta[E_2^+(\kappa,P,T)]\right\}\frac{q_\perp|J_{N+1,N'}(u)|^2}{a_{\ell\eta}^{\lambda}q_\perp^2+\frac{b_{\ell\eta}^{\lambda}}{L_z^2}}dq_\perp, \end{aligned} \tag{37} $$

where

$$ \begin{aligned} Y_1 \quad &= [1+N_{\ell,q_\perp}(\kappa)] f_{N+1,n}(\kappa,P,T)[1-f_{N',n'}(\kappa,P,T)] \\ &\quad -N_{\ell,q_\perp}(\kappa) f_{N',n'}(\kappa,P,T)[1-f_{N+1,n}(\kappa,P,T)], \end{aligned} \tag{38} $$

$$ \begin{aligned} Y_2 \quad &= N_{\ell,q_\perp}(\kappa) f_{N+1,n}(\kappa,P,T)[1-f_{N',n'}(\kappa,P,T)] \\ &\quad -[1+N_{\ell,q_\perp}(\kappa)] f_{N',n'}(\kappa,P,T)[1-f_{N+1,n}(\kappa,P,T)], \end{aligned} \tag{39} $$

$$ \begin{aligned} Y_3 \quad &= [1+N_{\ell,q_\perp}(\kappa)] f_{N',n'}(\kappa,P,T)[1-f_{N,n}(\kappa,P,T)] \\ &\quad -N_{\ell,q_\perp}(\kappa) f_{N,n}(\kappa,P,T)[1-f_{N',n'}(\kappa,P,T)], \end{aligned} \tag{40} $$

$$ \begin{aligned} Y_4 \quad &= N_{\ell,q_\perp}(\kappa) f_{N',n'}(\kappa,P,T)[1-f_{N,n}(\kappa,P,T)] \\ &\quad -[1+N_{\ell,q_\perp}(\kappa)] f_{N,n}(\kappa,P,T)[1-f_{N',n'}(\kappa,P,T)], \end{aligned} \tag{41} $$

$$ \begin{aligned} E_1^{\pm}(\kappa,P,T) \quad &= \quad \hbar\omega + (n^{'}-n)\hbar\omega_z + (N^{'}-N-1)\hbar\omega_c(\kappa,P,T) \\ &\quad \pm\hbar\omega_{LO}^{\ell,q_\perp}(\kappa), \end{aligned} $$

$$ E_2^{\pm}(\kappa,P,T) = \hbar\omega + (n-n^{'})\hbar\omega_z + (N-N^{'})\hbar\omega_c(\kappa,P,T) \pm \hbar\omega_{LO}^{\ell,q_\perp}(\kappa), $$

$$ \delta[E_1^{\pm}(\kappa,P,T)] = \frac{1}{\pi}\frac{\gamma_{N,N'}^{\pm}(\kappa,P,T)}{[E_1^{\pm}(\kappa,P,T)]^2+[\gamma_{N,N'}^{\pm}(\kappa,P,T)]^2}, \tag{42} $$

$$ \delta[E_2^{\pm}(\kappa,P,T)] = \frac{1}{\pi}\frac{\gamma_{N+1,N'}^{\pm}(\kappa,P,T)}{[E_2^{\pm}]^2+[\gamma_{N+1,N'}^{\pm}(\kappa,P,T)]^2}, \tag{43} $$

where

$$[\gamma^{\pm}_{N',N}(\kappa,P,T)]^2 = \frac{e^2}{8\pi^2\hbar^2\varepsilon_0 V_0}\left[N_{\ell,q_\perp}(\kappa)+\frac{1}{2}\pm\frac{1}{2}\right] \sum_{\ell}\sum_{\theta=\pm}\hbar\omega^{\ell,q_\perp}_{LO}(\kappa)|Y^{\ell\theta}_{nn'}|^2 \times\int_0^\infty q_\perp dq_\perp \frac{|J_{N,N'}(u)|^2}{a^{\lambda}_{\ell\eta}q_\perp^2+\frac{b^{\lambda}_{\ell\theta}}{L_z^2}}, \tag{44}$$

$$[\gamma^{\pm}_{N+1,N'}(\kappa,P,T)]^2 = \frac{e^2}{8\pi^2\hbar^2\varepsilon_0 V_0}\left[N_{\ell,q_\perp}(\kappa)+\frac{1}{2}\pm\frac{1}{2}\right] \sum_{\ell}\sum_{\theta=\pm}\hbar\omega^{\ell,q_\perp}_{LO}(\kappa)|Y^{\ell\theta}_{nn'}|^2 \times\int_0^\infty q_\perp dq_\perp \frac{|J_{N+1,N'}(u)|^2}{a^{\lambda}_{\ell\theta}q_\perp^2+\frac{b^{\lambda}_{\ell\eta}}{L_z^2}}, \tag{45}$$

According to the analytical results of Eq. (14), in the Huang-Zhu and guided mode models with even confinement modes, and in the slab mode model with odd confinement modes which contribute to the $0\rightarrow 0$ transition. Meanwhile, in the Huang-Zhu and guided mode models with odd confined modes, and in the slab modes model with even confinement modes which contribute to the $0\rightarrow 1$ transition, namely:

For the HZ model, we have.

When n and n' are even/odd, then we have

$$Y^{\ell,-}(nn') = \sqrt{\frac{n!2^{n-n'}}{n'!}}\left[\exp(-\frac{\ell^2\pi^2a_z^2}{4L_z^2})L_n^0(\frac{\ell^2\pi^2a_z^2}{2L_z^2})-(-1)^{\ell/2}\right], \quad \ell = 2,4,6,\cdots. \tag{46}$$

When n' and n respectively are even and odd, or vice versa, then we have

$$Y^{\ell,-}(nn') = 0,\ \ell = 2,4,6,\cdots. \tag{47}$$

When n and n' respectively are odd and even, or vice versa, then we have

$$Y^{\ell,+}(nn') = \sqrt{\frac{n!2^{n-n'}}{n'!}}\left[\frac{\mu_\ell\pi a_z}{L_z}\exp(-\frac{\mu_\ell^2\pi^2a_z^2}{4L_z^2})L_n^1(\frac{\mu_\ell^2\pi^2a_z^2}{2L_z^2})+(n+1)\frac{c_\ell a_z}{L_z}\right], \quad \ell = 3,5,7,\cdots. \tag{48}$$

When n and n' are even or odd, then we have

$$Y^{\ell,+}(nn') = 0,\ \ell = 3,5,7,\cdots. \tag{49}$$

For the slab mode model, we have.

When n' and n respectively are even and odd, or vice versa, then we have

$$Y^{\ell,-}(nn') = \sqrt{\frac{n!2^{n-n'}}{n'!}}\left(\frac{\ell\pi a_z}{L_z}\right)\exp(-\frac{\ell^2\pi^2a_z^2}{4L_z^2}) L_n^1(\frac{\ell^2\pi^2a_z^2}{2L_z^2}),\ \ell = 2,4,6,\cdots. \tag{50}$$

When n and n' together are even (odd), then we obtain

$$Y^{\ell,-}(nn') = 0,\ \ell = 2,4,6,\cdots. \tag{51}$$

When n and n' together are even (odd), the we obtain

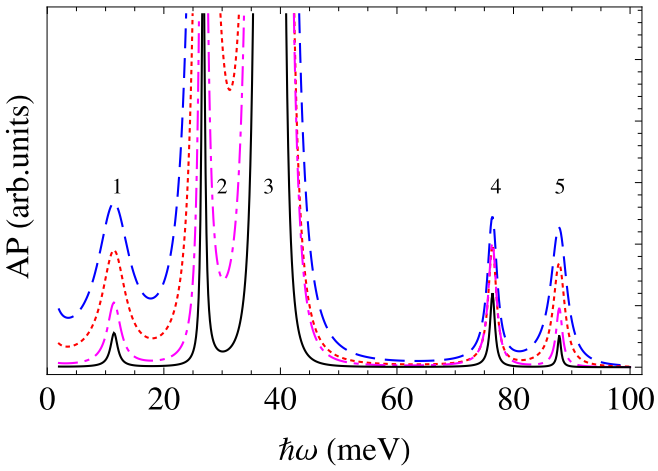

Fig. 1. The magneto-optical AP in GaAs/$Ga_{1-\kappa}Al_\kappa$As parabolic potential quantum wells as a function of $\hbar\omega$ (energy of photon) for all four kinds of various phonon modes: bulk modes (the black solid curve), guided modes (the magenta dashed-dotted curve), slab modes (the red dotted-dotted curve), and HZ model (the blue dashed-dashed curve) at temperature of system $T = 300$ K, hydrostatic pressure $P = 2$, and Al-contents $\kappa = 0.3$ GPa. (For interpretation of the references to colour in this figure legend, the reader is referred to the Web version of this article.)

$$Y^{\ell,+}(nn') = \sqrt{\frac{n!2^{n-n'}}{n'!}}\exp(-\frac{\ell^2\pi^2a_z^2}{4L_z^2})L_n^0(\frac{\ell^2\pi^2a_z^2}{2L_z^2}),\ \ell = 1,3,5,\cdots. \tag{52}$$

When n' and n respectively are even and odd, or vice versa, then we have

$$Y^{\ell,+}(nn') = 0,\ \ell = 1,3,5,\cdots. \tag{53}$$

For the guided mode model, we have.

When n' and n respectively are even and odd, or vice versa, then we have

$$Y^{\ell,-}(nn') = 0,\ \ell = 2,4,6,\cdots. \tag{54}$$

When n and n' are even/odd, then we have

$$Y^{\ell,-}(nn') = \sqrt{\frac{n!2^{n-n'}}{n'!}}\exp(-\frac{\ell^2\pi^2a_z^2}{4L_z^2})L_n^0(\frac{\ell^2\pi^2a_z^2}{2L_z^2}),\ \ell = 2,4,6,\cdots. \tag{55}$$

When n and n' respectively are odd and even, or vice versa, then we have

$$Y^{\ell,+}(nn') = \sqrt{\frac{n!2^{n-n'}}{n'!}}\left(\frac{\ell\pi a_z}{L_z}\right)\exp(-\frac{\ell^2\pi^2a_z^2}{4L_z^2}) L_n^1(\frac{\ell^2\pi^2a_z^2}{2L_z^2}),\ \ell = 1,3,5,\cdots. \tag{56}$$

When n and n' are even/odd, then we have

$$Y^{\ell,+}(nn') = 0,\ \ell = 1,3,5,\cdots. \tag{57}$$

Based on these analytical results, we present the numerical result and discussions in Sec. 4.

4. Results and discussions

Assuming only following levels are occupied by electron: $N = 0$, $N' = 1$ and $n = 0$, $n' = 0, 1$. Our results for effect of Al contents κ, temperature T, and pressure P on the FWHM and AP in GaAs/$Ga_{1-\kappa}Al_\kappa$As wells are presented and discussed in detail at the electron confining frequency $\omega_z = 0.3\omega_{LO}$ and the value of magnetic field B satisfies the magnetophonon resonance condition.

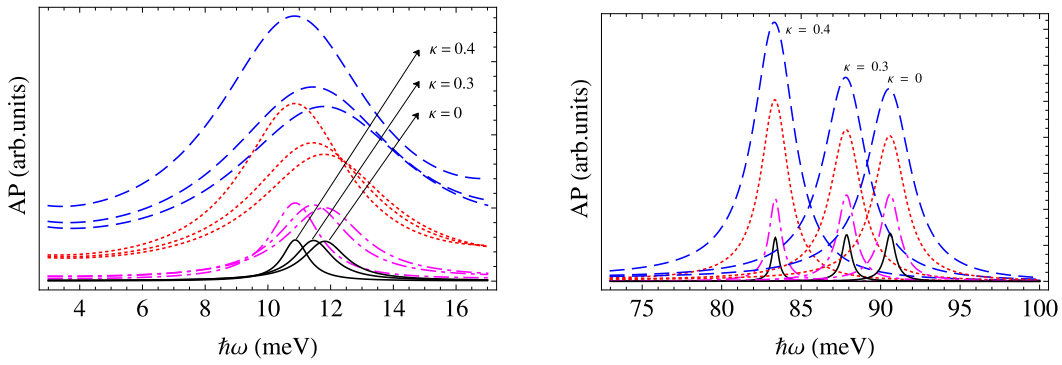

Fig. 2. The magneto-optical AP as a function of $\hbar\omega$ at phonon absorption (left Fig.) and emission (right Fig.) peaks with different Al-contents of GaAs/$Ga_{1-\kappa}Al_\kappa$As PQWs for all four kinds of different phonon modes: bulk modes (the black solid curve), guided modes (the magenta dashed-dotted curve), slab modes (the red dotted-dotted curve), and HZ model (the blue dashed-dashed curve). Here, $T = 300$ K, $P = 2$ GPa. (For interpretation of the references to colour in this figure legend, the reader is referred to the Web version of this article.)

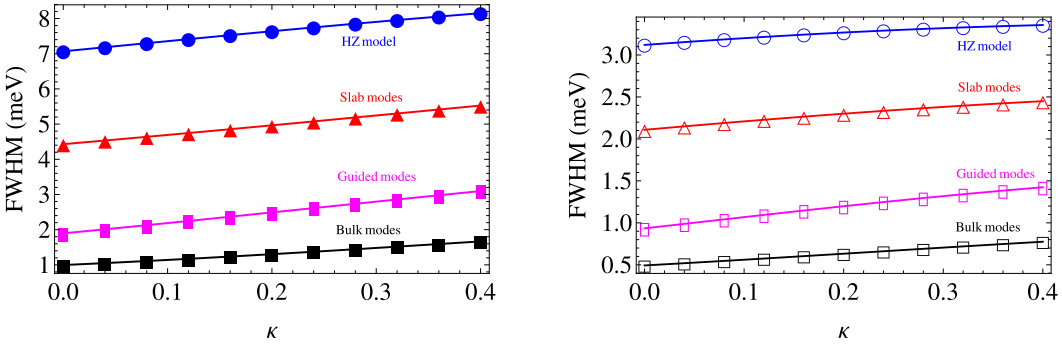

Fig. 3. Variation of the FWHM with Al contents κ of the phonon absorption process (left Fig.) and phonon emission process (right Fig.) for all four kinds of various phonon modes (bulk, guided, slab, HZ) in GaAs/$Ga_{1-\kappa}Al_\kappa$As PQWs. Here $T = 300$ K, $P = 2$ GPa.

Fig. 1 indicates five peaks numbered from (1) to (5). Peaks (1) and (5) locate at photon energies are 11.46 (meV) and 87.86 (meV), respectively. These peaks are called the ODMPR peaks because they accord with conditions that $\hbar\omega = (n' - n)\hbar\omega_z + (N' - N)\hbar\omega_c(\kappa, P, T) \mp \hbar\omega_{LO}(\kappa)$. It indicates that electron move from $n = 0$ to 1 together with $N = 0$ to 1 due to $\hbar\omega$-absorption along with $\hbar\omega_{LO}(\kappa)$-absorption/emission. Peak (2) is at photon energy, 26.74 (meV), and is called the ODMPR peak due to it accords with condition $\hbar\omega = (n - n')\hbar\omega_z\hbar\omega_{LO}(\kappa)$. This indicates that electron move from $0 \to 1$ of n levels caused by absorption of $\hbar\omega$ together with $\hbar\omega_{LO}(\kappa)$-emission. (3) peak locates at energy 38.20 (meV). It describes the transition intra-electric subbands because it accords with condition $\hbar\omega = \hbar\omega_{LO}(\kappa)$. (4) peak is at energy 76.40 (meV). This peak is called the ODMPR peak because it accords with following conditions: $\hbar\omega = (N' - N)\hbar\omega_c(\kappa, P, T) + \hbar\omega_{LO}(\kappa)$. It refers to the electron transition from $0 \to 1$ of N levels because of absorption of $\hbar\omega$ together with $\hbar\omega_{LO}(\kappa)$-emission.

Fig. 2 represents the AP intensity of phonon absorption/emission peak rises with aluminum concentration κ under all bulk phonon and confined phonon is due to Al-contents effects on the AP intensity through the factors $N_{\vec{q}}(\kappa)$ and $[1 - f_{N',n'}(\kappa, P, T)]f_{N,n}(\kappa, P, T)$. Meanwhile the position of the resonance peak shifts toward photon has lower energy. This can be explained that the Al contents explicit dependence of the arguments of Dirac delta functions in expressions (32), (32) and (42), (42).

Fig. 3 shows the FWHM of phonon absorption/emission peak which is displayed as function of composition κ under all bulk phonons and confinement phonons. This denotes the composition κ affects not only on the peak position, as well as AP intensity but also on the FWHM. Fig. 3 also displays that the FWHM slightly increases as composition κ increases under all phonon emission as well as absorption processes in all

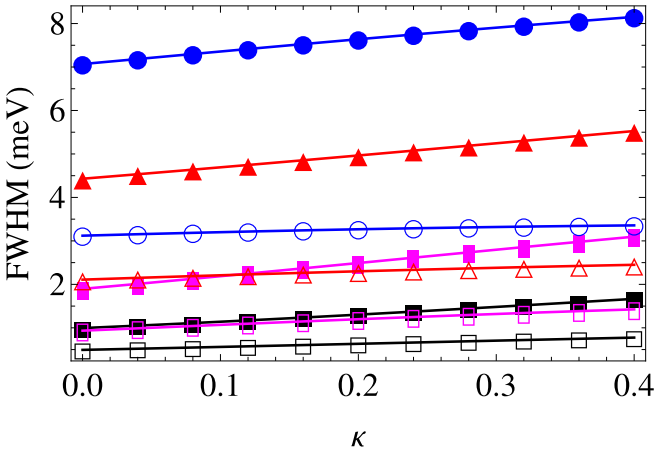

Fig. 4. Comparison of the value of FWHM and its variation with κ in GaAs/$Ga_{1-\kappa}Al_\kappa$As PQWs of the phonon mode absorption peak (blue filled circles (HZ model), red filled triangles (slab modes), magenta filled rectangles (guided modes), black filled squares (bulk modes) curves) with that of the phonon mode emission peak (blue empty circles (HZ model), red empty triangles (slab modes), magenta empty rectangles (guided modes), black empty squares (bulk modes) curves) for all four kinds of various phonon modes. Here, $T = 300$ K, $P = 2$ GPa. (For interpretation of the references to colour in this figure legend, the reader is referred to the Web version of this article.)

confinement phonons and bulk phonons cases by reason of the electrons–LO-phonons scattering probability increases as composition κ raises. Our obtained result is qualitative consistent with previous experimental

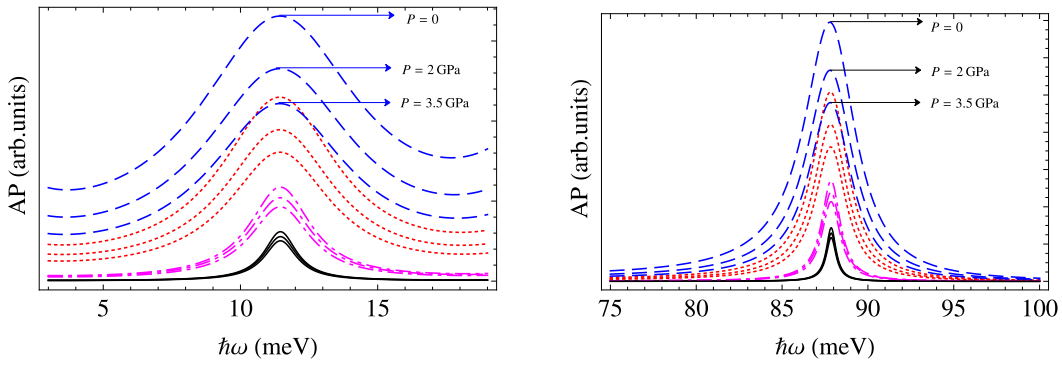

Fig. 5. The magneto-optical AP as a function of photon energy, $\hbar\omega$, at phonons absorption (left Fig.) and emission (right Fig.) peaks with different pressures in GaAs/$Ga_{1-\kappa}Al_\kappa As$ PQWs for all four kinds of different phonon modes: bulk modes (the black solid curve), guided modes (the magenta dashed-dotted curve), slab modes (the red dotted-dotted curve), and HZ model (the blue dashed-dashed curve). In which, $\kappa = 0.3$, $T = 300$ K. (For interpretation of the references to colour in this figure legend, the reader is referred to the Web version of this article.)

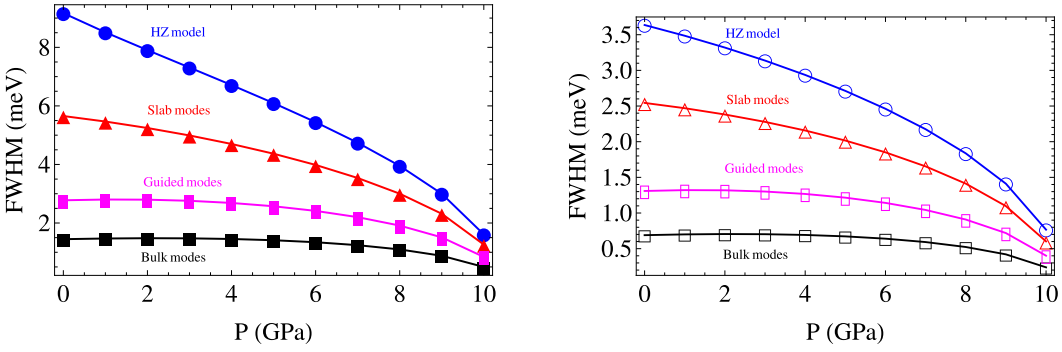

Fig. 6. Comparison of the value of the FWHM and its variation with pressure, P, at phonon absorption peak (left Fig.) and phonon emission peak (right Fig.) in GaAs/$Ga_{1-\kappa}Al_\kappa As$ PQWs for all four kinds of various phonon modes (bulk, guided, slab, HZ). Here, $\kappa = 0.3$, $T = 300$ K.

data in Refs. [11,61–63]. Specially, the value of the FWHM for the confined modes case is found to be always larger that for the bulk modes case under all absorption and emission of phonons. Because the confinement of phonons in parabolic wells leads to a decrease in scattering rate of electrophonon due to LO-phonons, i.e., the electron mobility increases, wherefore the electrons–LO-phonons scattering possibility raises. This is consistent with experimental result in Ref. [64].

We compare the value of the FWHMs and their variation with Al-contents, κ, of absorption-peak of phonon to those of emission-peak of phonon under all confined phonon and bulk phonon, as denoted clearly in Fig. 4. Our result represents the value of the FWHMs as well as their variation with Al-concentration κ for absorption-peak of phonon are much bigger as well as much faster than those of emission-peak of phonon for both bulk phonons and confinement phonons. For instance, the value of the FWHM at $\kappa = 0.3$ for phonon absorption process caused by HZ, slab modes, guided modes, and bulk modes models respectively is about 2.39, 2.26, 2.07, and 2.00 times as large as phonon emission process is. This implies that the electrophonon interaction caused by absorption of phonon is much stronger in comparison to that caused by emission of phonon for both four kinds of phonon modes. This is explained that the phonon absorption process leads to a increase of electron energy, the electron–phonon scattering rate decreases [65], i.e., the mobility of electron increases wherefore the electrophonon scattering possibility increases, i.e., the absorption FWHM rises [64]. The phonon-mode absorption dominates over phonon-mode emission in quantum wells here is good qualitative consistent with that obtained by scattering rates of electrophonon in quantum wires [66,67] and scattering rates of electron with confined phonon in wurtzite heterostructures [68]. However, this behaviour shows the difference between quantum well structures and monolayer MoS_2 [69] where the emission

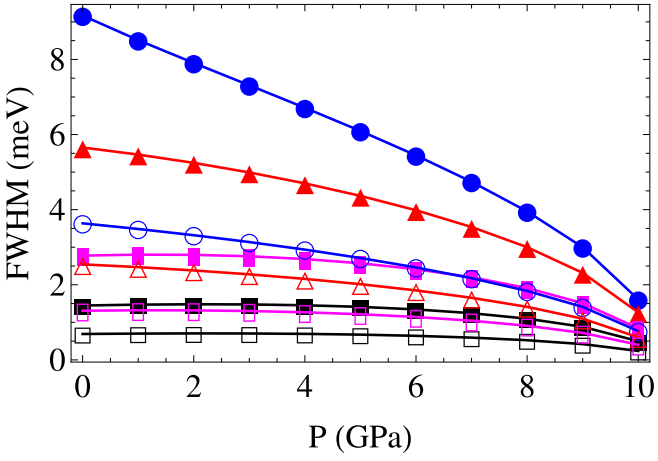

Fig. 7. Comparison of the value of the FWHM and its variation with P caused by the phonon mode absorption process (blue filled circles (HZ model), red filled triangles (slab modes), magenta filled rectangles (guided modes), black filled squares (bulk modes) curves) with that caused by the phonon mode emission process (blue empty circles (HZ model), red empty triangles (slab modes), magenta empty rectangles (guided modes), black empty squares (bulk modes) curves) for all four kinds of various phonon modes in GaAs/$Ga_{1-\kappa}Al_\kappa As$ PQWs. Here, $\kappa = 0.3$ and $T = 300$ K. (For interpretation of the references to colour in this figure legend, the reader is referred to the Web version of this article.)

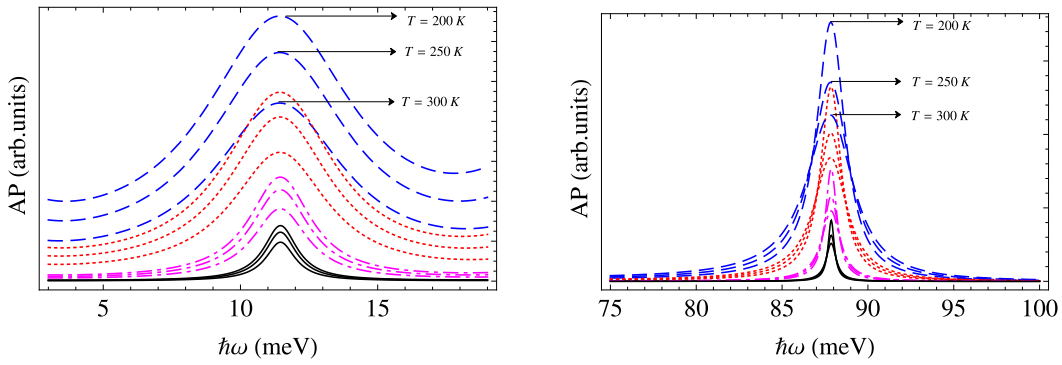

Fig. 8. The magneto-optical AP as a function of photon energy, $\hbar\omega$, at phonon absorption (left Fig.) and emission (right Fig.) peaks with different temperatures for GaAs/$Ga_{1-\kappa}Al_\kappa$As PQWs for all four kinds of different phonon modes: bulk modes (the black solid curve), guided modes (the magenta dashed-dotted curve), slab modes (the red dotted-dotted curve), and HZ model (the blue dashed-dashed curve). Where, $\kappa = 0.3$, $P = 2$ GPa. (For interpretation of the references to colour in this figure legend, the reader is referred to the Web version of this article.)

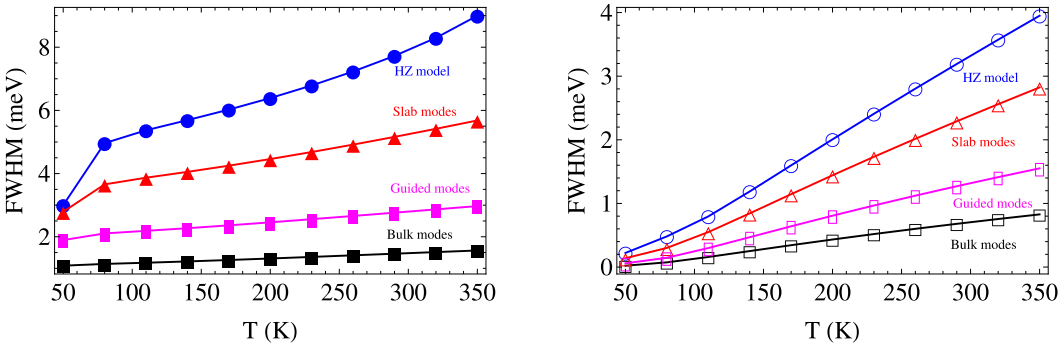

Fig. 9. Variation of the FWHM with T of the absorption of phonon (left Fig.) and phonon emission (right Fig.) for all four kinds of various phonon modes (bulk, Guided, Slab, HZ) in GaAs/$Ga_{1-\kappa}Al_\kappa$As PQWs. Here, $\kappa = 0.3$, $P = 2$ GPa.

process of phonon-mode is always more dominant than absorption process of phonon-mode.

Fig. 5 indicates that the AP intensity of the peak with phonon absorption as well as that of the peak with phonon emission decreases with the hydrostatic pressure P for all bulk and confined modes because of the hydrostatic pressure effects on the AP intensity by the factor $f_{N,n}(\kappa, P, T)$ $[1 - f_{N',n'}(\kappa, P, T)]$. However, the position of the peak remains unchanged with variation of the pressure P.

Fig. 6 shows the FWHM as a function of P in two bulk phonons and confinement phonons cases under all emission and absorption of phonon modes. The FWHM vigorously decreases as P increases under all four cases of phonons (confinement phonon and bulk phonon; emission and absorption of phonons). This result can be physically explained by a reduction in electrons–LO-phonons scattering possibility, in other words the electron mobility decreases as hydrostatic pressure increases. Especially for the confined phonon, the FWHM is always biggest and it fastest reduces for the HZ model while smallest and slowest reduce for the guided modes model. This refers to the electrophonon scattering is strongest with Huang-Zhu model but weakest with guided mode model among three different models of the confinement phonon (HZ, slab, and guided models). It is good consistent with previous results of Bhat et al. [70,71], in which who showed that the Huang and Zhu model which has been wide accepted and it best describes the electrophonon scattering in 2D structures. On the other hand, our results may be useful to orient for experimental consideration in the future [72–74], where they showed that only the confined phonons model which proposed by HZ agrees both quantitatively and qualitatively with experimental results.

Comparison of the value of the FWHM and its variation with hydrostatic pressure, P, of emission-peak of phonon with that of absorption-peak of phonon in two cases of confinement phonons and bulk phonons, as described in Fig. 7. The figure also indicates the value of FWHM and its variation with P of emission-peak of phonon are always much smaller and much slower than absorption-peak of phonon under

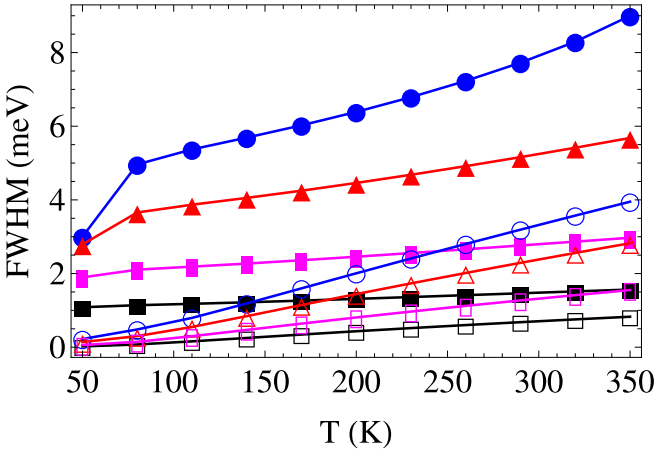

Fig. 10. Comparison of the value of the FWHM and its variation with T due to the phonon mode absorption (blue filled circles (HZ model), red filled triangles (slab modes), magenta filled rectangles (guided modes), black filled squares (bulk modes) curves) with that due to the phonon mode emission (blue empty circles (HZ model), red empty triangles (slab modes), magenta empty rectangles (guided modes), black empty squares (bulk modes) curves) for all four kinds of various phonon modes in GaAs/$Ga_{1-\kappa}Al_\kappa$As PQWs. Here, $\kappa = 0.3$ and $P = 2$ GPa. (For interpretation of the references to colour in this figure legend, the reader is referred to the Web version of this article.)

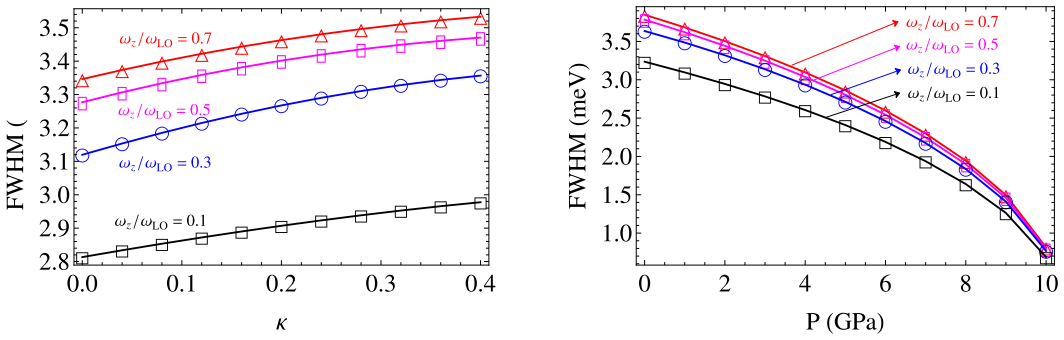

Fig. 11. Comparison of the value of the FWHM and its variation with κ (left Fig.) and hydrostatic pressure P (right Fig.) at various values of the electron confining frequency ω_z in GaAs/$Ga_{1-\kappa}Al_\kappa$As PQWs for confined phonons described by Huang-Zhu. Here, $T = 300$ K, $P = 2$ GPa and $\kappa = 0.3$, respectively.

all confinement phonons and bulk phonons. This refers to the intensity of phonon scattering for phonon emission process is much weaker compared to that for phonon absorption process under all four kinds of above phonon modes. This result is found to be in qualitative agreement with that obtained by scattering rates of electron with confined mode in wurtzite heterostructures [68].

Fig. 8 shows that with increasing temperature T, the position of the resonance peak remains unchanged. However, the AP intensity of the phonon absorption/emission peak decreases under all bulk phonon and confined phonon is due to temperature effects on the AP intensity by the factors $N_{\underset{q}{-}}(\kappa)$ and$[1 - f_{N',n'}(\kappa, P, T)]f_{N,n}(\kappa, P, T)$.

Fig. 9 shows the variation of FWHMs for phonon absorption/emission peaks with T for all four types of different phonon modes models (bulk, guided, slab, HZ models) in GaAs/$Ga_{1-\kappa}Al_\kappa$As parabolic quantum wells at $\kappa = 0.3$ and $P = 2$ GPa. We can see from Fig. 9 that the FWHMs increase with rising T under all bulk phonons and confinement phonons is because of the FWHM is proportional to the electrophonon scattering probability which is enhanced when increasing temperature T. Our obtained results are in good qualitative agreement with experimental data in Refs. [61,75–80]. In particular, the FWHMs caused by phonon confinement of the HZ model which are found to fastest increase and have a largest value among three different modes kinds of phonons confinement (HZ, slab modes, and guided modes models), as clearly illustrated in Fig. 9. This implies that the electron interaction with confined mode is strongest for the HZ model while that is weakest for the guided modes model.

Effect of T on the FWHM of phonon absorption-peak is compared to that of phonon emission peak at $\kappa = 0.3$ and $P = 2$ GPa in GaAs/$Ga_{1-\kappa}Al_\kappa$As parabolic quantum wells under all two kind of modes of phonon (bulk phonon and confined phonon), as indicated clearly in Fig. 10. The Fig. also shows the absorption of phonon modes is more dominant in comparison to emission of phonon modes, and in particular, for phonons confinement, the more pronounced this property is. Also, the strength of the electrophonon scattering is strongest for confined mode absorption which described by HZ model among four type of above modes.

Fig. 11 shows the variation of FWHM with κ (left figure) and P (right figure) at different confining frequencies of electron, ω_z, in GaAs/$Ga_{1-\kappa}Al_\kappa$As PQWs for confined mode which described by HZ model. We can see from the figures that the FWHMs always increase with increasing electron-confining frequency ω_z. However, for variation of FWHM with P (right figure), the rise of the FWHM with ω_z is slight and it becomes saturated rapidly at large confining frequency of electron ($\omega_z \geq 0.5\omega_{LO}$) in comparison to that for the variation of the FWHM with κ (left figure). This implies that the hydrostatic pressure weakly depends on the electron confining frequency in GaAs/$Ga_{1-\kappa}Al_\kappa$As parabolic quantum wells while the Al-concentration strongly depends on that, as clearly shown in left figure.

5. Conclusions

Magneto-optical transport properties of GaAs/$Ga_{1-\kappa}Al_\kappa$As parabolic wells under the combined influences of temperature, Al-concentration, and hydrostatic pressure have been studied. Using the projection operator and profile methods to analytically and numerically calculate the absorption power and FWHM, respectively. The obtained results show that (i) the FWHMs slightly increase with increasing aluminum concentration, temperature, but decrease with increasing hydrostatic pressure for both emission and absorption of phonons under all confined phonon and bulk phonon; (ii) the value of the FWHMs and their variation for phonon absorption process are fair bigger and much faster than those for phonon emission process under all confined phonon and bulk phonon, i.e., the intensity of electron–phonon scattering for phonon emission process is much weaker compared to that for phonon absorption process under all four types of above modes; (iii) the value of FWHMs for confined modes case is found to be always larger that for bulk modes case under all phonon modes emission and absorption, i.e., the strength of the electron–phonon scattering for confined modes is stronger in comparison to that for bulk modes under all two processes of phonon, and that is strongest for confined mode described by HZ model; (iv) the FWHMs always increase with increasing electron-confining frequency ω_z; (v) the increase of the FWHM with electron-confining frequency is slight and becomes saturated at large confining frequency of electron ($\omega_z \geq 0.5\omega_{LO}$) in GaAs/$Ga_{1-\kappa}Al_\kappa$As parabolic quantum wells; (vi) the aluminum concentration strongly depends on the electron confining frequency compared to hydrostatic pressure. We hope these results can be useful for the photonic and optoelectronic device fabrication.

CRediT authorship contribution statement

Le Thi Quynh Huong: Software, Investigation, Validation, Writing - original draft, Writing - review & editing. **Le Ngoc Minh:** Conceptualization, Methodology, Software, Investigation, Funding acquisition, Writing - original draft. **Nguyen Thi Xuan Hoai:** Methodology, Investigation, Funding acquisition, Writing - original draft. **Nguyen Dinh Hien:** Software, Methodology, Investigation, Conceptualization, Supervision, Writing - original draft, Writing - review & editing.

Declaration of competing interest

The authors declare that they have no known competing financial interests or personal relationships that could have appeared to influence the work reported in this paper.

References

[1] W. Xu, F.M. Peeters, J.T. Devreese, Phys. Rev. B 48 (1993) 1562.
[2] S.C. Lee, Y.B. Kang, D.C. Kim, J.Y. Ryu, N.L. Kang, S.D. Choi, Phys. Rev. B 55 (1997) 6719.

[3] S.C. Dhanabalan, B. Dhanabalan, J.S. Ponraj, Q. Bao, H. Zhang, Adv. Opt. Mater. 5 (19) (2017) 1700257.
[4] L. Lu, X. Tang, R. Cao, L. Wu, Z. Li, G. Jing, B. Dong, S. Lu, Y. Li, Y. Xiang, J. Li, D. Fan, H. Zhang, Adv. Opt. Mater. 5 (17) (2017) 1700301.
[5] Y. Zhang, C.-K. Lim, Z. Dai, G. Yu, J.W. Haus, H. Zhang, P.N. Prasad, Phys. Rep. 795 (2019) 1.
[6] X. Jiang, A.V. Kuklin, A. Baev, Y. Ge, H. Ågren, H. Zhang, P.N. Prasad, Phys. Rep. 848 (2020) 1–58.
[7] C. Xing, J. Zhang, J. Jing, J. Li, F. Shi, Chem. Eng. J. 370 (2019) 120.
[8] N.D. Vy, H.T. Cao, D.B.T. Thoai, H. Haug, Phys. Rev. B 80 (2009) 195306.
[9] J. Pei, J. Yang, T. Yildirim, H. Zhang, Y. Lu, Adv. Mater. 31 (2) (2019) 1706945.
[10] S. Guo, Y. Zhang, Y. Ge, S. Zhang, H. Zeng, H. Zhang, Adv. Mater. 31 (39) (2019) 1902352.
[11] S. Adachi, J. Appl. Phys. 58 (3) (1985) R1.
[12] X. Qi, Y. Zhang, Q. Ou, S.T. Ha, C.-W. Qiu, H. Zhang, Y.-B. Cheng, Q. Xiong, Q. Bao, Small 14 (31) (2018) 1800682.
[13] L. Wu, Y. Dong, J. Zhao, D. Ma, W. Huang, Y. Zhang, Y. Wang, X. Jiang, Y. Xiang, J. Li, Y. Feng, J. Xu, H. Zhang, Adv. Mater. 31 (14) (2019) 1807981.
[14] A. Svizhenko, A. Balandin, S. Bandyopadhyay, M.A. Stroscio, Phys. Rev. B 57 (1998) 4687.
[15] S. Rudin, T.L. Reinecke, Phys. Rev. B 41 (1990) 7713.
[16] C.R. Bennett, K. Güven, B. Tanatar, Phys. Rev. B 57 (1998) 3994.
[17] S. Yu, K.W. Kim, M.A. Stroscio, G.J. Iafrate, A. Ballato, Phys. Rev. B 50 (1994) 1733.
[18] Y.J. Cho, S.D. Choi, Phys. Rev. B 49 (1994) 14301.
[19] J.Y. Sug, S.G. Jo, J. Kim, J.H. Lee, S.D. Choi, Phys. Rev. B 64 (2001) 235210.
[20] H. Kobori, T. Ohyama, E. Otsuka, J. Phys. Soc. Jpn. 59 (6) (1990) 2141.
[21] D. Dunn, A. Suzuki, Phys. Rev. B 29 (1984) 942.
[22] T.C. Phong, H.V. Phuc, Mod. Phys. Lett. B 25 (12n13) (2011) 1003.
[23] N.D. Hien, Phys. E Low-dimens. Syst. Nanostruct. 114 (2019) 113608.
[24] L.T.T. Phuong, L. Dinh, N.D. Hien, J. Phys. Chem. Solid. 136 (2020) 109127.
[25] N.D. Hien, Superlattice. Microst. 131 (2019) 86.
[26] K.D. Pham, L. Dinh, P.T. Vinh, C. Duque, H.V. Phuc, C.V. Nguyen, Superlattice. Microst. 120 (2018) 738.
[27] K. Doan Quoc, H. Nguyen Dinh, Opt. Quant. Electron. 51 (4) (2019) 116.
[28] K.D. Pham, L.V. Tung, D.V. Thuan, C.V. Nguyen, N.N. Hieu, H.V. Phuc, J. Appl. Phys. 126 (12) (2019) 124301.
[29] N.D. Hien, Optik 206 (2020) 164348.
[30] K.D. Pham, L. Dinh, C.V. Nguyen, N.N. Hieu, P.T. Vinh, L.T.N. Tu, H.V. Phuc, Appl. Phys. A 125 (3) (2019) 166.
[31] N.D. Hien, C. Duque, E. Feddi, N.V. Hieu, H.D. Trien, L.T. Phuong, B.D. Hoi, L. T. Hoa, C.V. Nguyen, N.N. Hieu, H.V. Phuc, Thin Solid Films 682 (2019) 10.
[32] C.V. Nguyen, N.N. Hieu, N.A. Poklonski, V.V. Ilyasov, L. Dinh, T.C. Phong, L. V. Tung, H.V. Phuc, Phys. Rev. B 96 (2017) 125411.
[33] N. Binh, B.D. Hoi, D.V. Thuan, N.N. Hieu, C.V. Nguyen, H.V. Phuc, T.S. Tien, N. T. Nhan, N.D. Hien, N.N. Anh, L.T. Dung, L.T. Phuong, J. Phys. Chem. Solid. 125 (2019) 74.
[34] N.D. Hien, C.V. Nguyen, N.N. Hieu, S.S. Kubakaddi, C.A. Duque, M.E. Mora-Ramos, L. Dinh, T.N. Bich, H.V. Phuc, Phys. Rev. B 101 (2020), 045424.
[35] S.Y. Choi, S.C. Lee, H.J. Lee, H.S. Ahn, S.W. Kim, J.Y. Ryu, Phys. Rev. B 66 (2002) 155208.
[36] N. Mori, T. Ando, Phys. Rev. B 40 (1989) 6175.
[37] D.J. Barnes, R.J. Nicholas, F.M. Peeters, X.-G. Wu, J.T. Devreese, J. Singleton, C.J. G.M. Langerak, J.J. Harris, C.T. Foxon, Phys. Rev. Lett. 66 (1991) 794.
[38] G.-Q. Hai, F.M. Peeters, Phys. Rev. B 60 (1999) 16513.
[39] E. Reyes-Gómez, N. Raigoza, L.E. Oliveira, Phys. Rev. B 77 (2008) 115308.
[40] N. Raigoza, C.A. Duque, E. Reyes-Gómez, L.E. Oliveira, Phys. Status Solidi 243 (3) (2006) 635.
[41] U. Venkateswaran, M. Chandrasekhar, H.R. Chandrasekhar, T. Wolfram, R. Fischer, W.T. Masselink, H. Morkoç, Phys. Rev. B 31 (1985) 4106.
[42] E. Kasapoglu, F. Ungan, H. Sari, I. Sökmen, Phys. E Low-dimens. Syst. Nanostruct. 42 (5) (2010) 1623.
[43] M.A. Afromowitz, J. Appl. Phys. 44 (3) (1973) 1292.
[44] S.C. Lee, J.W. Kang, H.S. Ahn, M. Yang, N.L. Kang, S.W. Kim, Phys. E Low-dimens. Syst. Nanostruct. 28 (4) (2005) 402.
[45] S.C. Lee, J. Kor. Phys. Soc. 51 (2007) 1979.
[46] H.V. Phuc, N.N. Hieu, L. Dinh, T.C. Phong, Optic Commun. 335 (2015) 37.
[47] J.S. Bhat, S.S. Kubakaddi, B.G. Mulimani, J. Appl. Phys. 70 (4) (1991) 2216.
[48] N. Kang, Y. Ji, H.J. Lee, S. Choi, J. Kor. Phys. Soc. 42 (2003) 379.
[49] N. Kang, Y. Lee, S. Choi, J. Kor. Phys. Soc. 44 (2004) 1535.
[50] P. Vasilopoulos, Phys. Rev. B 33 (1986) 8587.
[51] G.-Q. Hai, F.M. Peeters, Phys. Rev. B 60 (1999) 8984.
[52] J. Gong, X.X. Liang, S.L. Ban, J. Appl. Phys. 100 (2) (2006), 023707.
[53] K. Huang, B.-F. Zhu, Phys. Rev. B 38 (1988) 2183.
[54] K. Huang, B. Zhu, Phys. Rev. B 38 (1988) 13377.
[55] S. Rudin, T.L. Reinecke, Phys. Rev. B 41 (1990) 7713.
[56] B.K. Ridley, Phys. Rev. B 39 (1989) 5282.
[57] R. Fuchs, K.L. Kliewer, Phys. Rev. 140 (1965) A2076.
[58] J.J. Licari, R. Evrard, Phys. Rev. B 15 (1977) 2254.
[59] J.Y. Sug, S.G. Jo, J. Kim, J.H. Lee, S.D. Choi, Phys. Rev. B 64 (2001) 235210.
[60] M.P. Chaubey, C.M. Van Vliet, Phys. Rev. B 33 (1986) 5617.
[61] T. Unuma, M. Yoshita, T. Noda, H. Sakaki, H. Akiyama, J. Appl. Phys. 93 (3) (2003) 1586.
[62] M.A. Afromowitz, J. Appl. Phys. 44 (3) (1973) 1292.
[63] K.L. Campman, H. Schmidt, A. Imamoglu, A.C. Gossard, Appl. Phys. Lett. 69 (17) (1996) 2554.
[64] X.T. Zhu, H. Goronkin, G.N. Maracas, R. Droopad, M.A. Stroscio, Appl. Phys. Lett. 60 (17) (1992) 2141.
[65] A.M. Alcalde, G. Weber, Phys. Rev. B 56 (1997) 9619.
[66] S. Yu, K.W. Kim, M.A. Stroscio, G.J. Iafrate, A. Ballato, Phys. Rev. B 50 (1994) 1733.
[67] R. Mickevičius, V. Mitin, Phys. Rev. B 48 (1993) 17194.
[68] E.P. Pokatilov, D.L. Nika, A.A. Balandin, J. Appl. Phys. 95 (10) (2004) 5626.
[69] N.V.Q. Binh, Bui D. Hoi, Doan V. Thuan, Nguyen N. Hieu, Chuong V. Nguyen, Huynh V. Phuc, Tong S. Tien, Nguyen T.T. Nhan, Nguyen D. Hien, Nguyen N. Anh, Le T. Dung, Le T.T. Phuong, J. Phys. Chem. Solid. 125 (2019) 74.
[70] J.S. Bhat, B.G. Mulimani, S.S. Kubakaddi, Phys. Rev. B 49 (1994) 16459.
[71] J.S. Bhat, S.B. Kapatkar, S.S. Kubakaddi, B.G. Mulimani, Phys. Status Solidi 209 (1) (1998) 37.
[72] K.T. Tsen, K.R. Wald, T. Ruf, P.Y. Yu, H. Morkoç, Phys. Rev. Lett. 67 (1991) 2557.
[73] A. Seilmeier, H.-J. Hübner, G. Abstreiter, G. Weimann, W. Schlapp, Phys. Rev. Lett. 59 (1987) 1345.
[74] T. Ruf, K. Wald, P.Y. Yu, K. Tsen, H. Morkoç, K. Chan, Superlattice. Microst. 13 (2) (1993) 203.
[75] T. Unuma, T. Takahashi, T. Noda, M. Yoshita, H. Sakaki, M. Baba, H. Akiyama, Appl. Phys. Lett. 78 (22) (2001) 3448.
[76] P. von Allmen, M. Berz, G. Petrocelli, F.K. Reinhart, G. Harbeke, Semicond. Sci. Technol. 3 (12) (1988) 1211.
[77] P. Voisin, Y. Guldner, J.P. Vieren, M. Voos, P. Delescluse, N.T. Linh, Appl. Phys. Lett. 39 (12) (1981) 982.
[78] K. Muro, S. Mori, S. Narita, S. Hiyamizu, K. Nanbu, Surf. Sci. 142 (1) (1984) 394.
[79] M. Singh, Phys. Rev. B 35 (1987) 9301.
[80] B. Tanatar, M. Singh, Phys. Rev. B 43 (1991) 6612.